13th ewtec 2019 Proceedings of the 13th European Wave and Tidal Energy Conference 1-6 Sept 2019, Naples, Italy

A GPU-accelerated method for the hydrodynamic analysis of a biomimetic flapping-foil device for marine energy extraction

Panagiotis E. Koutsogiannakis, Evangelos S. Filippas, and Kostas A. Belibassakis

Abstract—**In the present work a biomimetic flapping-foil device is studied for the exploitation of marine renewable energy resources. For this purpose a GPU-accelerated Boundary Element Method (GPU-BEM), in its 3-dimensional version is developed. The lifting body is submerged far from the free surface, neglecting the interaction with the additional boundary. A Morino-type Kutta condition is imposed on the trailing edge and, by linearizing the trailing vortex sheet dynamics, a simplified wake model is used. However, the motion of the body and the initial shape of the wake are not linearized. The performance of various adaptive integration quadratures for the calculation of singular integrals emerging in BEM are also investigated. Different partitioning schemes are examined and the Richardson extrapolation technique is used to accelerate the convergence of the recursive quadrature routine. The developed numerical integration method is able to evaluate efficiently integrals with multiple singularities on N-dimensional hyper-cubes. The parallelization parameters that affect performance are determined and a mixed precision arithmetic scheme is used to optimize the performance of the algorithm. The concepts of polymorphism and inheritance, incorporated in object-oriented programming, encouraging the extension of the solver to treat different problems with similar structure in an elegant manner. The present method, after enhancement and further verification, can be applied to the design and control of such biomimetic devices extracting energy from waves and tidal currents nearshore.**

Keywords—**Ocean Renewable Energy, Flow energy harvester, Numerical modelling, Boundary Element Method, GPGPU programming, Adaptive integration quadratures.**

I. Introduction

TIDAL currents carry huge amounts of energy and their exploitation is a promising source of renewable energy. In recent years, various devices have been proposed for the exploitation of tidal energy. The majority of studied designs belong to the category of horizontal and vertical axis turbines [1]. Other designs include devices piezoelectric materials, VIV systems, sails and oscillating hydrofoils.

The idea to use an oscillating hydrofoil to extract energy from currents is not new. McKinney and DeLaurier [2] have proposed a device to harvest energy by oscillating wings and some first experiments were conducted by DeLaurier and Harris [3]. Parametric studies have been performed, i.e. [4], [5], [6], to map the performance of the power extraction for different pitching amplitudes and oscillation frequencies. Huxham et al. [5] report a maximum efficiency of 23.8% in their experiments.

Studies have shown that oscillating-hydrofoil energy devices, which exhibit similar operational characteristics as the biomimetic flapping-foil propulsors, have advantages over rotary turbines. The power extraction of horizontal axis turbine systems is constrained by the Betz limit. The theoretical maximum power horizontal axis turbines can extract during their operation is 59.3% of the power available in the water passing through the cross-section of the device, published independently by Betz [7], Lanchester [8] and Joukowsky [9]. This limit was corrected by Garrett and Cummins [10] to account for the constraint of the flow in a channel and the ratio of coverage of the channel cross-section with turbines. Garrett and Cummins [11] also note that the coverage of the channel with turbines in practice will be limited by navigational and ecological reasons.

Many researchers argue that energy harvesters utilizing oscillating hydrofoils can be more efficient than turbines and surpass the Betz limit; see e.g. Dabiri [12] and Young et al. [13]. This is attributed to the fact that flapping foils can take advantage of the unsteadiness of flow and vortex dynamics. The operational characteristics of the oscillating hydrofoils for marine energy harvesting are similar to the flapping-foils used for propulsion. More details on the performance parameters of flapping-foils can be found in the works Rozhdestvensky & Ryzhov [14] and Triantafyllou et al. [15].

Moreover, this behavior allows the oscillating foil to operate near the free-surface and extract energy from both waves and currents. In Filippas et al. [16], a numerical study was performed concerning an oscillating

1739 – Tidal Hydrodynamic Modelling

All authors share the same affiliation, School of Naval Architecture and Marine Engineering at the National Technical University of Athens, Heroon Polytechniou 9, Zografos 15773, Athens, Greece.
P. E. Koutsogiannakis (pkoutsogian@hotmail.com)
E. S. Filippas (evfilip@central.ntua.gr)
K.A. Belibassakis (kbel@fluid.mech.gr)

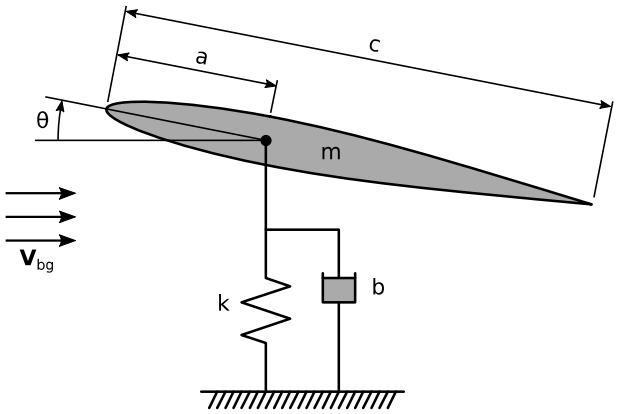

Fig. 1. Schematic of the semi-activated flapping foil.

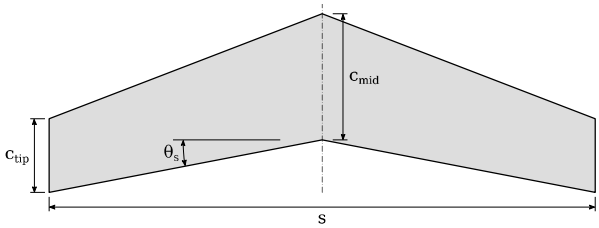

Fig. 2. Planform of hydrofoil. The foil is swept by an angle θ_s.

hydrofoil operating in waves, in the presence of sheared currents nearshore. It was demonstrated that a power efficiency of 53.5% can be achieved by using a single hydrofoil in harmonic pitching motion of amplitude $25°$.

Furthermore, the cumulative performance of oscillating hydrofoils in power production farms can be superior to that of turbine systems. Kinsey and Dumas [17] have reported a 59.9% efficiency for two flapping foils in a tandem configuration. This efficiency can reach values higher than 90% for 15 foils in tandem [18], while the total efficiency of turbines in similar configuration reaches asymptotically 66% [13].

Another aspect of tidal energy extraction systems that should be taken into account when proposing an energy harvesting solution is the ecological impact. The oscillating hydrofoils move slowly and as a result the noise pollution of such devices is limited. In contrast, the blade tips of horizontal axis turbines can reach high velocities and as a result they can be harmful for marine ecosystems.

Xiao & Zhu [19] classified those studies into three categories with respect to the activation mechanism of the flapping foil. The first category includes systems with prescribed rotational (pitching) and translatory (heaving) oscillatory motions of the foil, the second category includes semi-activated systems with forced pitching motion and induced heaving oscillations and the last one includes self-sustained systems with induced motions at both degrees of freedom.

In the present work, the 3D semi-activated oscillating foil device was studied to examine the potential for energy extraction. The device design can be seen in Figure 1. The current is assumed to have a uniform velocity distribution V_{bg}. The parameters, which affect the performance of the device, taken into consideration in the present work are the operational parameters and the geometry of the hydrofoil.

The foil has a chord length c and the pitching axis of the foil is located at a distance a from the leading edge. At first stage, a rectangular foil will be examined and next the effect of sweep angle (θ_s) will be examined. For the latter case a foil with linear distribution of the chord along the span will be studied. The planform of the swept foil can be seen in Figure 2.

For the hydrodynamic calculations a GPU-BEM was developed, extending our previous works ([16], [20]). For the efficient implementation of the numerical algorithm a computational code is developed, exploiting parallel programming techniques and general purpose programming on graphics processing units (GPGPU), by using the CUDA C/C++ application programming interface (API). The GPGPU programming alternative was chosen because modern GPUs have higher throughput of calculations than CPUs and at the same time are more efficient, i.e. 44 GFLOPS/Watt for an NVidia GTX Titan X, compared to 0.71 GFLOPS/Watt for Intel i7-8700K.

II. MATHEMATICAL FORMULATION

A. Oscillator

As a first approximation the free heaving motion of the semi-activated device with prescribed pitching motion, is modelled by a simple 1-degree-of-freedom damped oscillator described by the following equation

$$m\ddot{h} + b\dot{h} + kh = F_L(t) \tag{1}$$

Where h is the heave of the foil, m is the mass of the foil, b is the damping coefficient, modelling the energy generator, k is the spring coefficient, representing the elastic mount, and F_L is the lift generated by the oscillating foil on the earth-fixed coordinate system. The lift depends on the heave position (h) and the time derivative ($\dot{h}$), introducing an implicit non linearity to the problem.

The pitch angle (θ) of the foil is given as a periodic function of time (t). Here a sinusoidal profile will be assumed

$$\theta(t) = \theta_0 sin(\omega_p t) \tag{2}$$

where θ_0 is the amplitude of the pitching motion and ω_p is the angular frequency. Also, the reduced frequency is defined

$$f^* = \frac{fc}{V_{bg}} = \frac{\omega_p c}{2\pi V_{bg}} \tag{3}$$

The power consumed for the pitching motion is

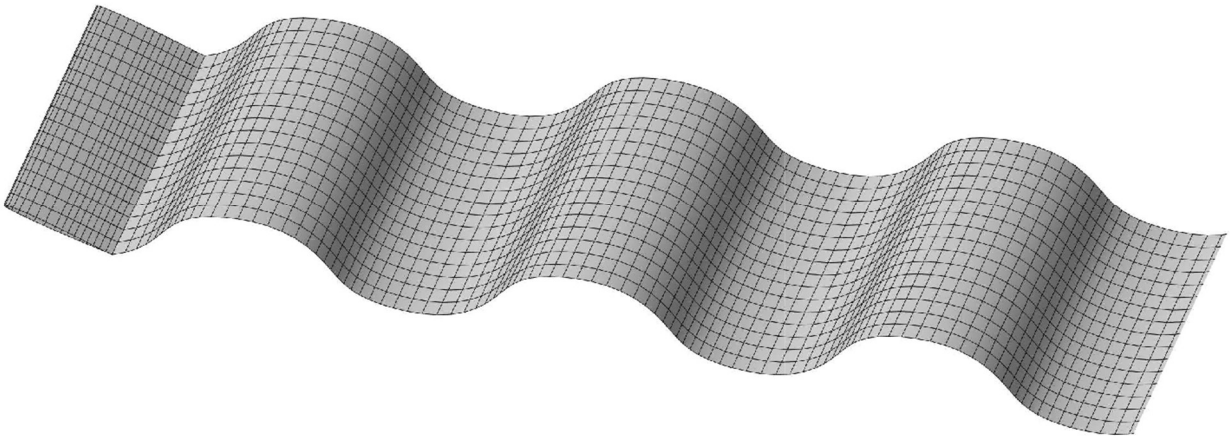

Fig. 3. Geometry discretization. The foil and wake boundaries are approximated with bilinear elements. The source and dipole distribution on the foil is considered piecewise constant.

$$P_{cons}(t) = M(t)\dot{\theta}(t) \tag{4}$$

where $M(t)$ is the moment producing the pitching motion. The power produced by the generator is

$$P_{prod}(t) = b\dot{h}^2(t) \tag{5}$$

The mean net power generated by the system in one period of the heaving motion is [19]

$$\bar{P}(t) = \int_{t}^{t+T} [b\dot{h}^2(\tau) - M(\tau)\dot{\theta}(\tau)]d\tau \tag{6}$$

and the efficiency of energy harvesting is

$$\eta = \frac{\bar{P}}{0.5\rho V_{bg}^3 Y_p s} \tag{7}$$

where Y_p is the difference between the highest and lowest points of the foil geometry in a period, s is the span of the foil and ρ is density of the fluid. The denominator represents the incoming flow kinematic energy flux. Defining the efficiency this way, will allow us to compare the performance of oscillating foils with turbines.

B. Lift Calculation

For the calculation of the hydrodynamic forces the Boundary Element Method is used. The device is assumed to operate submerged in an infinite domain (D). The fluid motion is modeled with the assumption of potential flow and the potential is defined to satisfy the equation

$$\Delta\Phi(\mathbf{x}) = 0, \mathbf{x} \in D \tag{8}$$

On the foil surface (∂D_B) the no-entrance boundary condition must be satisfied

$$\partial_{\mathbf{n}_B}\Phi(\mathbf{x}) = (\mathbf{V}(\mathbf{x}) - \mathbf{V}_{bg})\cdot\mathbf{n}_B \tag{9}$$

Where $\partial_{\mathbf{n}} = \mathbf{n}\cdot\nabla$ is the gradient of a function in the direction of vector **n, V** is the net velocity vector of the foil surface due to the heaving and pitching motions, V_{bg} $\boldsymbol{V}_{bg}$ is the current velocity vector and $\boldsymbol{n}_B$ is the unit normal vector to the boundary surface.

At large distance from the hydrofoil the disturbance field vanishes.

The wake (∂D_W) of the hydrofoil is modeled as a free shear layer surface. On this surface the kinematic and dynamic boundary conditions [21] are imposed as follows

$$\partial_{\mathbf{n}_W}\Phi^+(\mathbf{x}) = \partial_{\mathbf{n}_W}\Phi^-(\mathbf{x}), \mathbf{x} \in \partial D_W \tag{10}$$

$$p^+(\mathbf{x}) = p^-(\mathbf{x}), \mathbf{x} \in \partial D_W \tag{11}$$

In the equations above we denote with + the upper side of the wake and with – the lower side. These conditions, together with the Bernoulli's equation

$$\frac{\partial\Phi}{\partial t} + \frac{1}{2}(\nabla\Phi)^2 + \nabla\Phi\cdot\mathbf{V}_{bg} + \frac{p}{\rho} = 0 \tag{12}$$

result to

$$\frac{D\mu_W}{Dt}(\mathbf{x}) = 0, \mathbf{x} \in \partial D_W \tag{13}$$

Where $\mu_W = \Phi^+ - \Phi^-$ is the potential jump through the wake boundary and $\frac{D}{Dt} = \frac{\partial}{\partial t} + \boldsymbol{V}_W\cdot\nabla$ is the material derivative based on the mean total velocity of the wake $\boldsymbol{V}_W = \boldsymbol{V}_{bg} + (\nabla\Phi^+ + \nabla\Phi^-)/2$. This implies that the shear layer surface should move according to the total velocity ($\boldsymbol{V}_{bg} + \nabla\Phi$). In the present work a simplified wake model

is adopted, ignoring the effect of the disturbance potential on the motion of the wake surface; see e.g. [22].

In the case of lifting flow around sharp-ended hydrofoils, the problem is supplemented by the Kutta condition at the trailing edge. In the present work, a Morino-type Kutta condition will be used, demanding continuity of the potential at the trailing edge, as follows

$$\mu(TE)=\Phi^{+}(TE)-\Phi^{-}(TE) \tag{14}$$

where μ here is the dipole intensity generated at the trailing edge and transferred to the wake.

C. Boundary Integral Equation and Boundary Element Method

Using Green's representation theorem for points on the foil surface and the wake, we get the following relationship between the potential Φ on the hydrofoil and its derivative normal to the surface

$$\begin{aligned}&\frac{1}{2}\Phi_B(\mathbf{x})+\int_{\partial D_B}\Phi_B(\mathbf{y})\cdot\partial_{\mathbf{n}_B}G(\mathbf{x},\mathbf{y})dS(\mathbf{y})=\\&\int_{\partial D_B}G(\mathbf{x},\mathbf{y})\cdot\partial_{\mathbf{n}_B}\Phi_B(\mathbf{y})dS(\mathbf{y})-\int_{\partial D_W}\mu_W(\mathbf{y})\cdot\partial_{\mathbf{n}_W}G(\mathbf{x},\mathbf{y})dS(\mathbf{y})\end{aligned} \tag{15}$$

where G is the fundamental solution of the 3D Laplace equation

$$G(\mathbf{x},\mathbf{y})=-\frac{1}{4\pi||\mathbf{x}-\mathbf{y}||} \tag{16}$$

and represents the potential, at point $\mathbf{x}$, caused by a source of unit magnitude, placed on point $\mathbf{y}$.

The Boundary Integral Equation (BIE) (equation 15) is discretized according to BEM, by approximating the integration surfaces with bilinear elements (E_j) in a grid pattern; see Figure 3. The discrete system is derived by applying a collocation scheme to points ($\mathbf{x}_i$) coinciding with the centers of the elements on the foil surface. Here it should be noted that the last row of elements of the wake near the hydrofoil (Kutta strip) is always defined as the extension of the bisector surface of the trailing edge.

The Morino condition must be satisfied on the collocation points adjoin to the trailing edge. Denoting these collocation points with the subscript k^+ for the upper side and k^- for the lower side, the Morino condition can be written as

$$\mu_k=\Phi_{Bk^+}-\Phi_{Bk^-} \tag{17}$$

The discretized BIE and the Morino condition can be written together as

$$\begin{aligned}&\sum_{i=1}^{N_B}\left(\frac{\delta_{ij}}{2}+\sum_{k^+}\delta_{k^+j}B_{k^+j}-\sum_{k^-}\delta_{k^-j}B_{k^-j}+B_{ij}\right)\Phi_{Bj}=\\&\sum_{i=1}^{N_B}A_{ij}\left[(\mathbf{V}-\mathbf{V}_{bg})\cdot\mathbf{n}_B\right]_j+\sum_{j=1}^{N_W}(-B_{ij})\mu_{Wj}\end{aligned} \tag{18}$$

where A_{ij} and B_{ij} are the induced factors of source and dipole distributions respectively.

$$\begin{aligned}A_{ij}&=\int_{E_j}G(\mathbf{x}_i,\mathbf{y})dS(\mathbf{y})\\B_{ij}&=\int_{E_j}\partial_{\mathbf{n}}G(\mathbf{x}_i,\mathbf{y})dS(\mathbf{y})\end{aligned} \tag{19}$$

The disturbance velocity tangent to the foil surface is then calculated by a second order finite difference scheme.

Then the Bernoulli's equation (12) can be used to calculate the pressure on the foil surface. The pressure can then be integrated along the foil surface to calculate the forces acting on the hydrofoil.

D. Time integration and model coupling

By setting

$$\mathbf{z}=\begin{pmatrix}h\\\dot{h}\end{pmatrix}, \tag{20}$$

equation (1) can be written in a matrix form as

$$C\cdot\dot{\mathbf{z}}=D\cdot\mathbf{z}+\begin{pmatrix}F_L(t)\\0\end{pmatrix}=f(\mathbf{z}),C=\begin{pmatrix}b&m\\1&0\end{pmatrix},D=\begin{pmatrix}-k&0\\0&1\end{pmatrix} \tag{21}$$

By discretizing the above equation in time and applying a Crank-Nicholson scheme the equality that has to be satisfied at a given timestep is

$$C\cdot\dot{\mathbf{z}}^{t+\Delta t}=\frac{1}{2}(f(\mathbf{z}^{t+\Delta t})+f(\mathbf{z}^{t})) \tag{22}$$

We use an implicit Euler scheme and the time derivative of $\mathbf{z}$ can be approximated as follows

$$\dot{\mathbf{z}}^{t+\Delta t}=\frac{1}{\Delta t}(\mathbf{z}^{t+\Delta t}-\mathbf{z}^{t}) \tag{23}$$

and the system of equations becomes

$$\begin{aligned}&S(\mathbf{z}^{t+\Delta t})=\\&C\cdot(\mathbf{z}^{t+\Delta t}-\mathbf{z})-\frac{\Delta t}{2}(D\cdot\mathbf{z}^{t+\Delta t}+F_L^{t+\Delta t}+f(\mathbf{z}^{t}))=0\end{aligned} \tag{24}$$

This nonlinear system of equations is then solved using the Newton's method, as follows

$$\mathbf{z}_{n+1}^{t+\Delta t} = \mathbf{z}_{n}^{t+\Delta t} - J^{-1}(S)\cdot S(\mathbf{z}_{n}^{t+\Delta t}) \tag{25}$$

Where J is the Jacobian matrix of system S approximated by using second order central differences.

III. ADAPTIVE INTEGRATION ALGORITHM

The surface integrals arising in BEM are singular because there exists a collocation point in the domain of integration that coincides with a point on the integration domain. For this reason an adaptive integration algorithm is developed to facilitate the calculation of integrals for which an analytical solution is not known.

The adaptive integration routines can dynamically refine the interval of integration in order to get a better approximation near the singular points. A simple quadrature is used to obtain a first estimate of the integral, in the integration domain (Ω). Next, the interval is partitioned to m subintervals $\Omega_i, i = 1, \dots, m$, such that $\Omega = \cup\ \Omega_i$ and the simple quadrature is subsequently used on each subinterval. Then, the first estimation is compared to the sum of the subinterval estimations to determine the convergence. This procedure is repeated on every subinterval until a convergence criterion is satisfied.

The method relies on recursively integrating the function on smaller subdivisions of the initial domain. Lyness [23] studied an adaptive quadrature based on the simple Simpson's (1-4-1) rule. He proposed an accurate convergence criterion and modified the quadrature to include a term for convergence acceleration. Gander and Gautschi [24] present an adaptive quadrature based on the four-point Gauss-Lobatto rule with two successive Kronrod extensions.

In the present work, we propose an adaptive algorithm based on an N-point Gauss-Lobatto Quadrature with a uniform m-division strategy (GLQ_N).

The Richardson extrapolation technique [25] is used to increase the convergence rate of the recursive algorithm. For the Gauss-Lobatto quadrature of order N the error of the approximation is $O(h^{2N-2})$, where h here denotes the integration interval length, and for the adaptive routine with m uniform subdivisions at each recursion level the convergence can be accelerated by applying the Richardson extrapolation as

$$GLQ_N^{acc} = \frac{m^{2N-2} GLQ_N(h/m) - GLQ_N(h)}{m^{2N-2} - 1} + O(h^{2N-1}) \tag{26}$$

where GLQ_N^{acc} is the final accelerated estimation of the integral and GLQ_N is the non-accelerated result. Moreover, the arguments (h/m) and (h) of GLQ_N are the subdivision lengths for the current and the previous recursions respectively.

To evaluate singular surface integrals, it is important to have a very good approximation of the inner integral that bears the singularity. Then, the outer integration can be done by a lower order routine. In this way, the benefits of accuracy and robustness of the high order routine used for the inner integration are combined with the great speed of the simpler routine of the outer integration. Finally a fast and elegant routine for evaluating singular surface integrals is produced by using object oriented programming.

The adaptive routine can be generalized for integration over N-dimensional domains. By passing an adaptive integrator of (N-1) dimensions as an integrand function for the N-dimensional integrator and giving the N-th element of the position vector as a parameter, the routine will perform integrations recursively on all dimensions.

IV. GPU IMPLEMENTATION

E. GPU Performance Optimization

Modern GPUs have thousands of cores and as a result parallel algorithms can benefit greatly from that. More specifically, BEM is massively parallelizable, as the calculation of induced factors (single and double layer integrals) requires no inter-thread communication. The two operations that require the most computational time are the calculation of the single and double layer integral terms and the solution of the system to get the potential on collocation points. For the solution of the system the LU solver of cuBLAS library was used. Therefore, attention was given to the calculation of induced factors.

Two issues were identified that can have a major effect on GPU code performance. First, in order to achieve the maximum computational capacity of the GPU all the available CUDA cores must be used. There are many parameters that must be determined to accomplish the maximum occupancy of the GPU.

Initially, the workload of the threads within a block must be balanced. This means that the threads should take the same time to finish the scheduled work. If some threads need more time to execute, at the end of the kernel there will be less active warps, using only a subset of the cores.

The same is true about the unbalanced workload of blocks within a grid. In this case, limiting the size of the blocks and distributing the workload to more blocks will increase the efficiency of the algorithm, as new blocks will be launched at the time the previous ones will finish their execution.

Another problem can arise when too few blocks are launched on the GPU. If the number of blocks launched is less than the maximum number of blocks that can run simultaneously across all SMs then the occupancy is limited. The maximum number of blocks that can run at

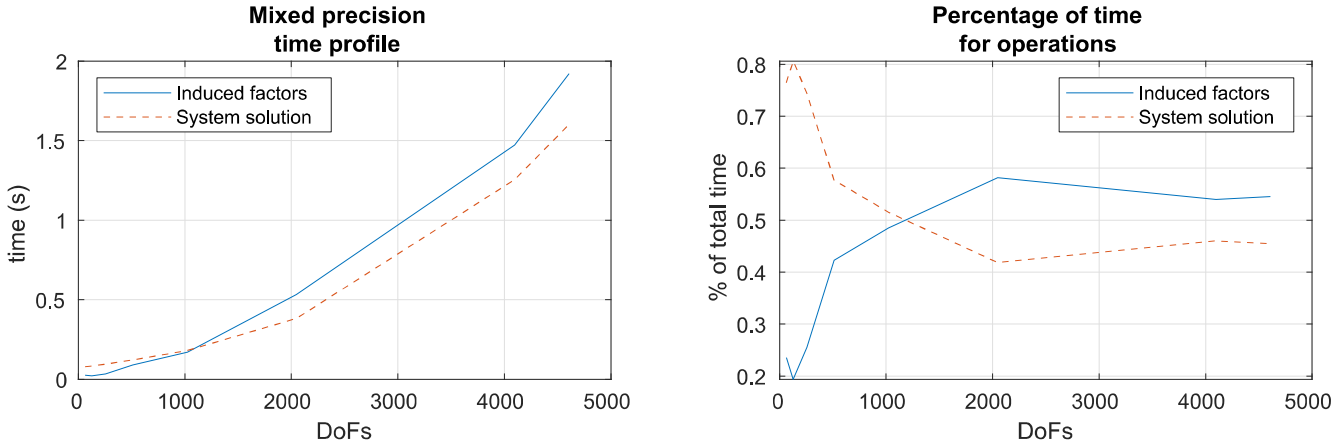

Fig. 4. Execution time profile for the calculation of the potential on the ellipsoid with semi-axis lengths $l_1 = 0.5$, $l_2 = 2.5$, $l_3 = 0.06$ and current velocity vector $V_{bg} = (-1,0,0)^T$. The calculation of the induced factors can be up to 58% of the total time for reasonable size systems.

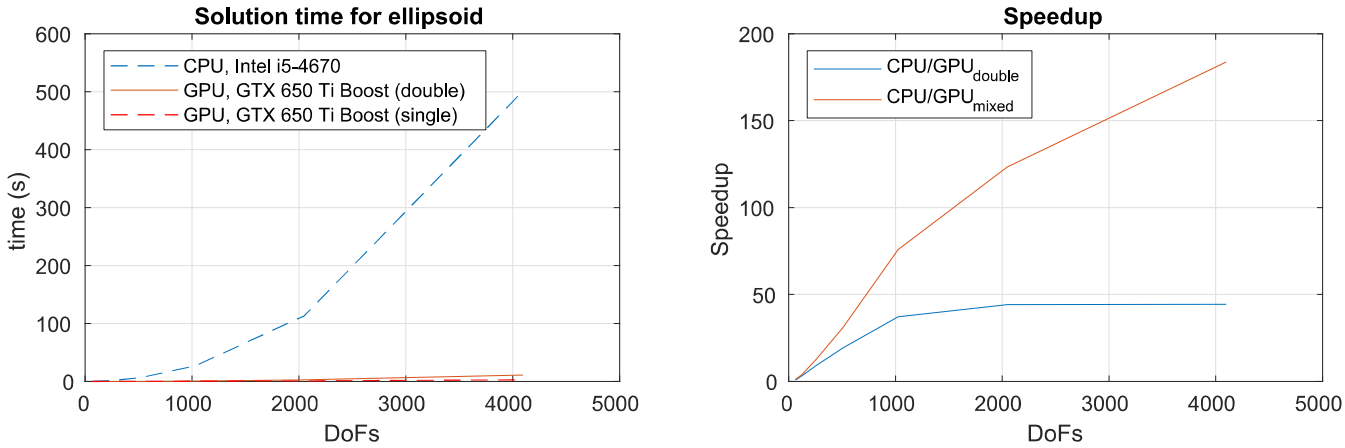

Fig. 5. Benchmarking between a single threaded CPU core (Intel i5-4670 3.4GHz) and an MSI GTX 650 Ti Boost GPU for the calculation of the potential on an ellipsoid, with semi-axis lengths $l_1 = 0.5$, $l_2 = 2.5$, $l_3 = 0.06$ and current velocity vector $V_{bg} = (-1,0,0)^T$. The calculation is accelerated 44 times using the GPU.

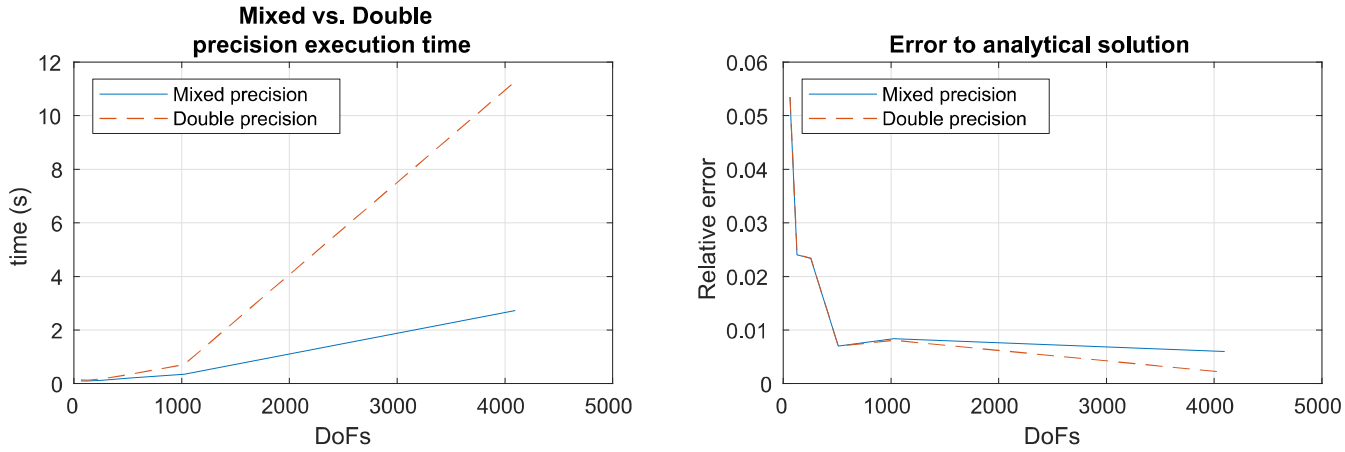

Fig. 6. Time for the calculation of the potential on an ellipsoid, with semi-axis lengths $l_1 = 0.5$, $l_2 = 2.5$, $l_3 = 0.06$ and current velocity vector $V_{bg} = (-1,0,0)^T$, and relative error to analytical solution [26]. With mixed precision the calculation is accelerated about 3-6 times, while the error for both cases converges to values less than 1%. The tests were performed on an NVidia GTX 650 Ti Boost.

once on the GPU is called a "full wave". When a kernel is launched with more blocks than a full wave then the blocks that cannot fit into a Streaming Multiprocessor (SM) will be scheduled for after another block has finished.

Moreover, each thread of a block will use the registers available to that block. This means that the limited register file must be adequate for all the threads of the block. To achieve this, the block size may need to be decreased or the register count per thread may be limited at compilation.

Finally, the last wave of operations scheduled may be partial and thus limit the occupancy. This means that for a problem that needs the last wave to be full, if other resources are adequate, the GPU resources will be used more efficiently than for a problem that will not occupy completely the GPU for the final block calculations.

The other problem that arises during implementation is memory coalescence. In order to maximize the efficiency of the algorithm the right data-structures should be chosen in order for threads of a warp running in parallel to access data that are spread in an as small as possible memory interval. In this way, we can take advantage of the hardware and use the complete bandwidth of the GPU memory.

Concerning the calculation of the single and double layer integrals with the adaptive routine, the computational workload becomes higher, the closer the collocation point is to the boundary element. This issue can affect the performance of the GPU kernel, as the threads that finish first will stall execution until all the threads have completed their respective tasks.

In the present work, the integrals are grouped depending on whether they are singular or not. More specifically, the diagonal elements (self-induced factors) of matrices A and B are calculated separately of the rest of the elements. Moreover, to decrease the computational complexity of self-induced factors calculation, a semi-analytical formula is used for the inner integration.

The method was tested for the calculation of the potential on the surface of an ellipsoid, with three principal axes parallel to the base vectors of the reference coordinate system, with half-lengths $l_1 = 0.5$, $l_2 = 2.5$, $l_3 = 0.06$ and the current velocity vector was $\boldsymbol{V}_{bg} = (-1,0,0)^T$. The results were then compared to the analytical solution [26]. In Figure 4, the total calculation time was analyzed to the individual operations. The two operations that require significant time are the calculation of the single and double layer terms and the solution of the produced linear system. It is shown that the calculation of the integrals takes up to 58% of the total time. The execution time as well as the memory footprint can be decreased by employing techniques like the Fast Multipole Method [27].

In Figure 5, the performance of the GPU code is compared with the performance of the code running on a single CPU thread. For the comparison, an Intel i5-4670 CPU and a single MSI GTX 650 Ti Boost GPU were used. The GPU completed the task up to 44 times faster than the CPU.

F. Mixed precision

As most commercially available GPUs have much more single precision throughput (FP32) than double precision throughput (FP64); e.g. the NVidia Pascal architecture SM has a FP32-to-FP64 performance ratio of 32. For this reason, it is preferred to perform calculations in single-precision arithmetic.

However, it was found that the single layer self-induced integral terms require double-precision, to yield the desired accuracy. Therefore, a mixed precision scheme is used; see e.g. [28]. The results can then be converted to single-precision and stored together with the induced potential factors calculated with single-precision arithmetic. The linear system is then solved using single-precision cuBLAS routines.

TABLE I
CONVERGENCE OF η FOR $\Delta t = T/128$

NEs/NEc	16	32	48
16	-0.0098	0.0316	0.0364
32	-0.0106	0.0312	0.0354
48	-0.0107	0.0305	0.0356

TABLE II
CONVERGENCE OF η FOR NES=32, NEC=48

Δt	T/32	T/64	T/128
-	0.0353	0.0353	0.0354

In Figure 6, the execution times for the calculation of the potential on the test ellipsoid, using the mixed precision scheme are compared with the same calculation using only double precision. The mixed precision is 6 times faster for fine grids and due to lower memory usage more demanding problems can be solved. It is significant that the error of the mixed precision remains close to that of double precision.

V. NUMERICAL RESULTS

G. Method convergence and validation

The present method was tested for a variety of grid sizes, to evaluate the convergence for different number of elements in the spanwise direction (NEs) and in the chordwise direction (NEc). The results are shown in table (I). In table (II) the convergence for smaller timesteps is shown. For the convergence tests, a rectangular foil was used, with NACA0005 cross section, c=1, AR=10 and a/c=0.5. The velocity of the current is assumed to be 1m/s, the reduced frequency of the motion is f*=1/π, the pitch amplitude is 10^o and the damping coefficient is b=10π. In this case the mass of the foil and the spring coefficient are ignored. In the following simulations the device parameters remain the same unless specified.

For NEs=32, NEc=48 and Δt=T/128 the method converges and those values will be used in the following simulations.

The present method is compared with the experiments of Huxham et al. [5]. In their experimental configuration, the hydrodynamic forces were transferred to a rotating shaft as a torque, through a swinging arm. Following the design of the experiment, a series of numerical simulations was performed. The foil has c=0.1m, a/c=0.25, the length of the swinging arm is r=0.3m and the current velocity is $V_{bg} = 0.5m/s$. The damping coefficient is equal to $b = 14.75\rho V_{bg} sc^2 r$ and not elastic connection (k=0). The mass of the foil was taken into consideration, in order to produce more accurate results. In Figure 7, the heaving amplitude of the pitch centre of the foil is plotted for reduced frequency $f^* = 0.1$ and various pitching amplitudes (ranging from 10 to 50 degrees). While in the

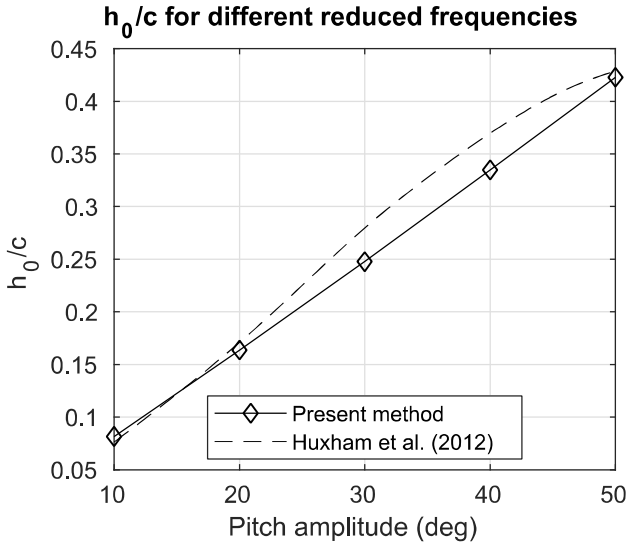

Fig. 7. : Heave amplitude comparison between the present method with corrections for resistance and the experiments conducted by Huxham et al. [5] for reduced frequency f* = 0.1.

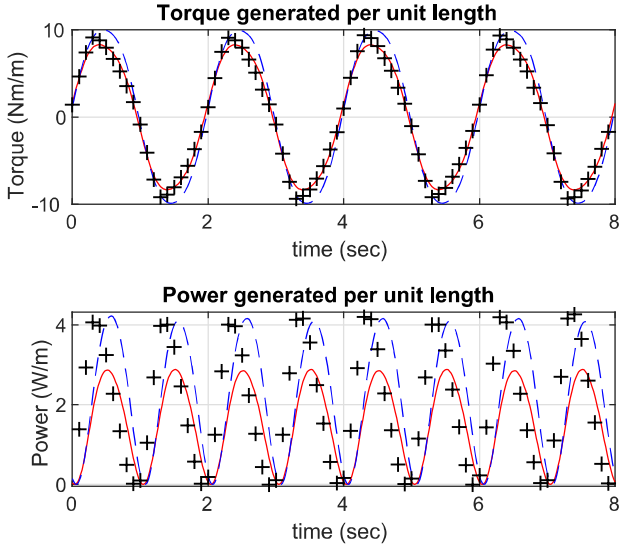

Fig. 8. : Torque output and power output timeseries between the present method and the experiments conducted by Huxham et al. [5] for f*= 0.1, θ_0= 50º and V_{bg}= 0.5. Crosses denote the experimental data, the solid line the results of the present method with AR=3.4 and the dashed line represents the results for AR=10.

experimental device the foil had AR=3.4, the foil used in the simulations has AR=10 to counteract the effect the plates at the wingtips have on the wake. In Figure 8, the effect of AR to the torque of the device and the net power output time series is shown, for $f^* = 0.1$, $\theta_0 = 50^o$ and $V_{bg} = 0.5m/s$. It is apparent that the power produced in the experiment is significantly higher that the results for the real aspect ratio of the foil. The output power increases in relation with the aspect ratio.

Discrepancies in the results can be attributed to the linearized quasi-steady Morino condition and linearized wake dynamics.

H. *Parametric study*

Next, a parametric study of the oscillating hydrofoil device is performed. For different distances of the pitch axis from the Leading Edge (a), the efficiency is determined for a range of damping coefficients and frequencies. The pitch amplitude is kept constant and equal to 50 degrees. More specifically, in Figure 9, the efficiency is plotted for a/c={0,0.25,0.5,0.75}, $b/\pi\rho csV_{bg} = 0-8$ and f*=0-0.7, where $\pi\rho csV_{bg}$ is the value of b for which the maximum efficiency for the 2D case occurs [29]. The foil has AR=10, c=1m, and the speed of the current is $V_{bg} = 1m/s$. The maximum performance is observed for f*=0.12 and $b/\pi\rho csV_{bg} = 1.12$, when the pitch axis is located at the mid-chord, and the corresponding efficiency is 0.232. For the different values of a/c examined, the location of the efficiency maximum varies slightly. These results are qualitatively similar to the results of Zhu et al. [29] for the 2D case. In the case of a/c=0.75, Zhu et al. [29] report a peculiar monotonic increase in performance with the frequency, however, in our simulations this behavior is not observed. It is apparent, though, that for a/c=0.75 the frequency range where energy extraction is achieved is wider than in the rest cases. Further investigation of that interesting behavior is left as a subject for future work.

Furthermore, in the work of Zhu et al. [29], for simplicity in the calculation, the efficiency is defined by dividing the net mean power extraction of the device by the power of the current through the rectangle defined by the span of the foil and the plunging amplitude. This definition can produce results that overestimate the efficiency of the foil. In Figure 10, this difference is depicted for different values of the pitching amplitude, for $b = \pi\rho csV_{bg}$, a/c=0.5 and $f^* = 1/\pi$. It is apparent that the more strict definition of efficiency (equation 7) is more suitable as a power coefficient for comparison with turbines and other devices. Moreover, the efficiency rises linearly with the pitch amplitude for all frequencies. This result is also observed by other researchers, i.e. [16], [29].

In Figure 11 the effect of a sweep angle and a linear chord distribution along the span of the hydrofoil is presented, for the parameters of the optimal rectangular hydrofoil. The geometry of the planform is determined by the sweep angle and the wing tip chord to middle chord ratio,$CR = c_{tip}/c_{mid}$, as seen in Figure 2. The sweep angle is varied from 0^o to 18^o in 6^o increments and the chord ratio from 0.2 to 1.0 in 0.1 increments. For the entire range of parameters tested, the sweep and CR<1 had a negative effect on efficiency.

I. *Comparison with turbines*

In order to compare the performance of oscillating hydrofoils with turbines, the equivalent Tip Speed Ratio (TSR_{eq}) for the hydrofoil is defined.

$$TSR_{eq} = \frac{\omega D_{eq}}{2V_{bg}} \tag{27}$$

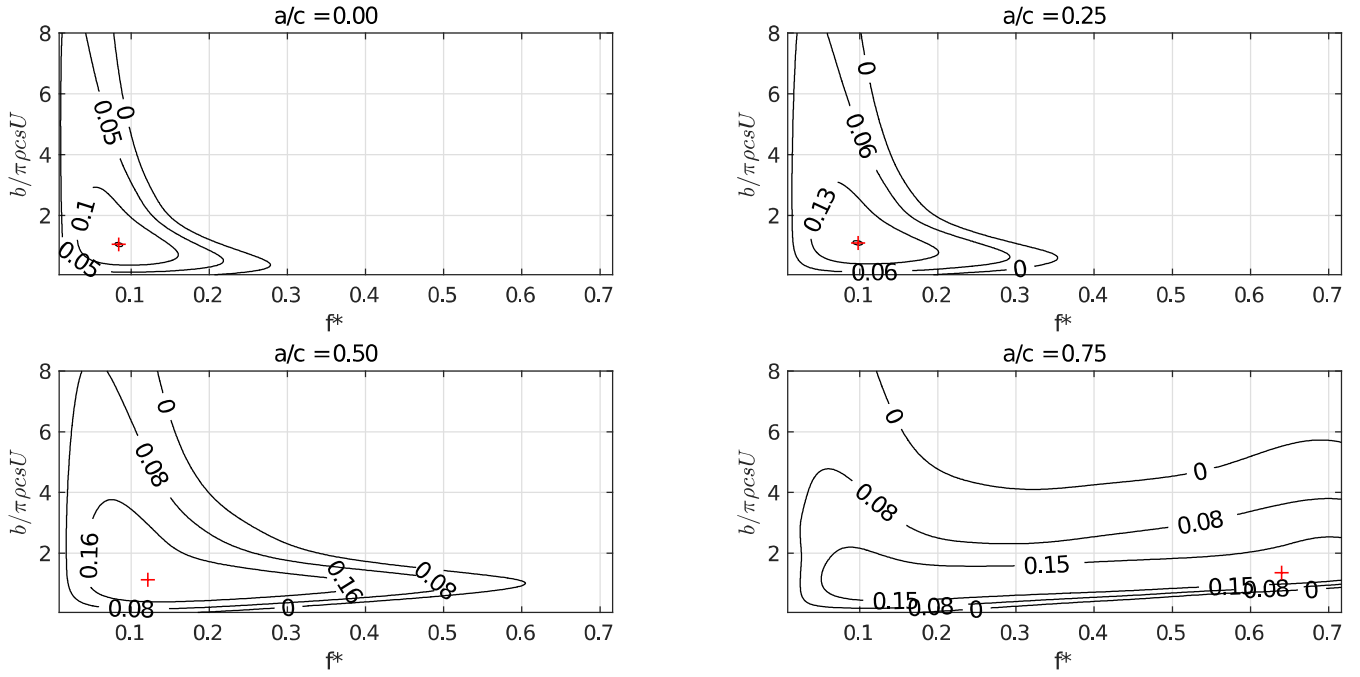

Fig. 9. Efficiency of the semi-activated flapping foil, plotted for a/c={0,0.25,0.5,0.75}, $b/\pi\rho scV_{bg}$=0-8, f*=0-0.7 and $\theta_0 = 50^o$. The maximum efficiency is observed at a/c=0.5, $b/\pi\rho csV_{bg}$=1.12 and f*=0.12. Crosses refer to points of maximum efficiency.

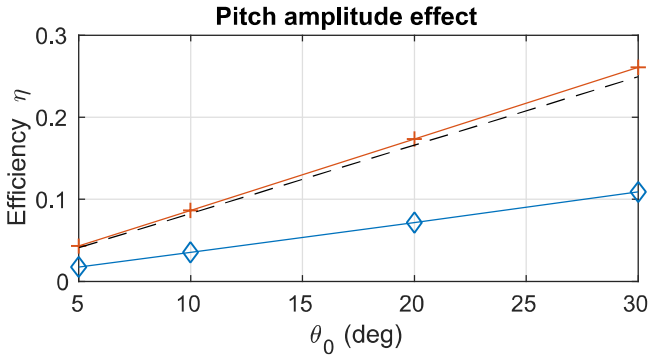

Fig. 10. Effect of pitch amplitude on the efficiency of the device. The efficiency rises linearly with the pitch amplitude. The dashed lines represent the results of Zhu et al. (2009), the line with crosses the results of the present method with efficiency defined by the plunging amplitude and the lines with diamonds show the efficiency calculated by equation 7.

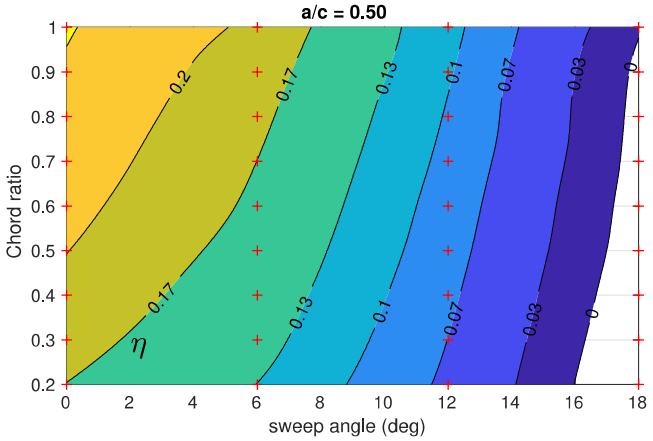

Fig. 11. Effect of the planform parameters on the efficiency of the device. Crosses refer to simulation points.

where

$$D_{eq} = \sqrt{4sY_p/\pi} \tag{28}$$

is the equivalent diameter of a circular disk with the same area as the sweep area of the oscillating hydrofoil and $\omega = 2\pi f^* V_{bg}/c$ the angular frequency of the oscillation.

Figure 12 shows the performance of the optimal oscillating hydrofoil, as derived from the simulation results, compared to the performance of a horizontal axis turbine. The data for the turbine are referenced from [30], for a model turbine in a cavitation tank, with hub pitch angle 20^o and current velocity $V_{bg} = 1m/s$. The oscillating hydrofoil device operates at lower TSR values than the turbine and peak efficiency occurs at TSR_{eq}=1.5.

VI. CONCLUSION

Oscillating hydrofoils are investigated as novel biomimetic systems for exploitation of marine renewable energy. The present method, based on BEM, is GPU-accelerated and the calculation of integrals is performed by a fast and elegant quadrature routine for evaluating singular surface integrals implemented using object oriented programming. A mixed precision scheme is used for utilising the maximum performance of the GPU. The validity of the present method is tested with experimental data. Numerical results concerning the operating parameters of the oscillating hydrofoil device are presented. Furthermore, the oscillating hydrofoil device is compared to proposed tidal turbines. The present method can be useful for the design and control of such devices. Future work includes the extension of the method with a more accurate model for the trailing edge treatment and a more complex wake model. Also, it is

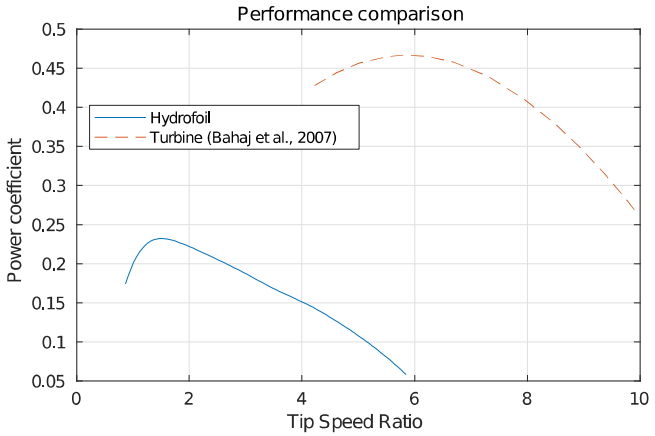

Fig. 12. Comparison of oscillating hydrofoil performance with horizontal axis turbine. The oscillating hydrofoil yields peak efficiency at lower frequencies than the turbine.

significant to investigate the performance of such biomimetic systems in multicomponent configurations. For this purpose, a modern high performance computing (HPC) code, that scales well on a GPU cluster, will be developed. That will be achieved by the combination of CUDA API with the message passing interface (MPI).

ACKNOWLEDGEMENT

Support of E. Filippas by Alexander S. Onassis Public Benefit Foundation scholarship is acknowledged.

REFERENCES

[1] M. J. Khan, G. Bhuyan, M. T. Iqbal and J. E. Quaicoe, "Hydrokinetic energy conversion systems and assessment of horizontal and vertical axis turbines for river and tidal applications: a technology status review," *Applied energy,* vol. 86, no. 10, p. 1823–1835, 2009.

[2] W. McKinney and J. DeLaurier, "Wingmill: an oscillating-wing," *Journal of energy,* vol. 5, no. 2, p. 109–115, 1981.

[3] J. D. DeLaurier and J. M. Harris, "Experimental study of oscillating-wing," *Journal of Aircraft,* vol. 19, no. 5, p. 368–373, 1982.

[4] T. Kinsey and G. Dumas, "Parametric study of an oscillating airfoil in a power-extraction regime," *AIAA journal,* vol. 46, no. 6, p. 1318–1330, 2008.

[5] G. H. Huxham, S. Cochard and J. Patterson, "Experimental parametric investigation of an oscillating hydrofoil tidal stream energy converter," *18th Australasian Fluid Mechanics Conference (AFMC), Launceston, Australia,* 3-7 December 2012.

[6] Q. Zhu, "Optimal frequency for flow energy harvesting of a flapping foil," *Journal of fluid mechanics,* vol. 675, p. 495–517, 2011.

[7] A. Betz, "Das maximum der theoretisch möglichen ausnutzung des windes durch windmotoren," *Z. Gesamte Turbinenwesen,* vol. 26, 1920.

[8] F. W. Lanchester, "A contribution to the theory of propulsion and the screw propeller," *Transactions of the Institution of Naval Architects,* vol. 57, pp. 98-116, 1915.

[9] N. E. Joukowsky, "Windmill of the NEJ type," *Transactions of the Central Institute for Aero-Hydrodynamics of Moscow,* 1920.

[10] C. Garrett and P. Cummins, "The efficiency of a turbine in a tidal channel," *Journal of fluid mechanics,* pp. 243--251, 2007.

[11] C. Garrett and P. Cummins, "Limits to tidal current power," *Renewable Energy,* vol. 33, no. 11, pp. 2485-2490, 2008.

[12] J. O. Dabiri, "Renewable fluid dynamic energy derived from aquatic animal locomotion," *Bioinspiration & biomimetics,* vol. 2, no. 3, p. L1, 2007.

[13] J. Young, J. C. Lai and M. F. Platzer, "A review of progress and challenges in flapping foil power generation," *Progress in Aerospace Sciences,* vol. 67, p. 2–28, 2014.

[14] K. V. Rozhdestvensky and V. A. Ryzhov, "Aerohydrodynamics of flapping-wing propulsors," *Progress in Aerospace Sciences,* vol. 39, no. 8, pp. 585-633, 2003.

[15] M. S. Triantafyllou, A. H. Techet and F. S. Hover, "Review of experimental work in biomimetic foils," *IEEE Journal of Oceanic Engineering,* vol. 29, no. 3, pp. 585-594, 2004.

[16] E. S. Filippas, T. P. Gerostathis and K. A. Belibassakis, "Semi-activated oscillating hydrofoil as a nearshore biomimetic energy system in waves and currents," *Ocean Engineering,* vol. 154, p. 396–415, 2018.

[17] T. Kinsey and G. Dumas, "Optimal tandem configuration for oscillating foils hydrokinetic turbine," *Journal of fluids engineering,* vol. 134, no. 3, 2012.

[18] H. R. Karbasian, J. A. Esfahani and E. Barati, "Simulation of power extraction from tidal currents by flapping foil hydrokinetic turbines in tandem formation," *Renewable Energy,* p. 816–824, 2015.

[19] Q. Xiao and Q. Zhu, "A review on flow energy harvesters based onflapping foils," *Journal of fluids and structures,* vol. 46, p. 174–191, 2014.

[20] E. S. Filippas and K. A. Belibassakis, "Hydrodynamic analysis of flapping-foil thrusters operating beneath the free surface and in waves," *Eng. Anal. Bound. Elements,* vol. 41, pp. 47-59, 2014.

[21] G. K. Politis, "Simulation of unsteady motion of a propeller in a fluid including free wake modeling," *Engineering Analysis with Boundary Elements,* vol. 28, no. 6, pp. 633-653, 2004.

[22] G. K. Politis, "Unsteady wake rollup modeling using a molifier based filtering technique," *Dev. Appl. Ocean Eng.,* vol. 5, pp. 1-28, 2016.

[23] J. N. Lyness, "Notes on the adaptive simpson quadrature routine," *J. ACM,* vol. 16, no. 3, p. 483–495, 1969.

[24] W. Gander and W. Gautschi, "Adaptive quadrature—revisited," *BIT Numerical Mathematics,* vol. 40, no. 1, p. 84–101, 2000.

[25] Richardson and Gaunt, "Viii. the deferred approach to the limit," *Philosophical Transactions of the Royal Society of London A: Mathematical, Physical and Engineering Sciences,* vol. 226, p. 299–361, 1927.

[26] M. Thomson and L. Melville, Theoretical Hydrodynamics, 1968.

[27] N. Nishimura, "Fast multipole accelerated boundary integral equation," *Applied mechanics reviews,* vol. 55, no. 4, p. 299–324, 2002.

[28] X. S. Trompoukis, "Solving aerodynamic-aeroelastic problems on Graphics Processing Units," *PhD thesis, School of Mechanical Engineering, National Technical University of Athens, Greece,* 2012.

[29] Q. Zhu, M. Haase and H. C. Wu, "Modeling the capacity of a novel flow-energy harvester," *Applied Mathematical Modelling,* vol. 33, no. 5, p. 2207–2217, 2009.

[30] A. S. Bahaj, A. F. Molland, J. R. Chaplin and W. M. J. Batten, "Power and thrust measurements of marine current turbines under various hydrodynamic flow conditions in a cavitation tunnel and a towing tank," *Renewable Energy,* vol. 32, p. 407–426, 2007.